Proceedings of the Institution of Civil Engineers
Bridge Engineering 158
September 2005 Issue BE3
Pages 107–115

Paper 14018
Received 08/11/2004
Accepted 12/05/2005

Keywords:
concrete structures/stress analysis/ thermal effects

Qing Xu
Capita Symonds,
East Grinstead, UK

Chris Burgoyne
Department of Engineering,
University of Cambridge, UK

ice

Thermal-creep analysis of concrete bridges

Q. Xu MPhil, GMICE and C. Burgoyne MA, MSc, PhD, DIC, CEng, MICE, FIStructE

The creep effects on sequentially built bridges are analysed by the theory of thermal creep. Two types of analysis are used: time dependent and steady state. The traditional uniform creep analysis is also introduced briefly. Both simplified and parabolic normalising creep–temperature functions are used in the analysis for comparison. Numerical examples are presented, calculated by a computer program based on the theory of thermal creep and using the displacement method. It is concluded that different assumptions within thermal creep can lead to very different results when compared with uniform creep analysis. The steady-state analysis of monolithically built structures can serve as a limit to evaluate total creep effects for both monolithically and sequentially built structures. The importance of the correct selection of the normalising creep–temperature function is demonstrated.

NOTATION

GCS Global coordinate system
LCS Local coordinate system
TTS Temperature-transformed section
Dotted symbols (e.g. $\dot{x}$) refer to differentiation of x with respect to pseudo-time.
Delta symbols (e.g. Δx) relate to increments of x.
Dashed symbols (e.g. x') relate to the local coordinate system of the temperature-transformed section.
Barred symbols (e.g. $\bar{x}$) relate to the local member coordinate system.
Subscript th (e.g. x_{th}) relates to thermal effects.
Subscript cr (e.g. x_{cr}) relates to creep effects.
Subscript ref (e.g. x_{ref}) relates to the reference state.
Subscript o (e.g. x_0) relates to the time of loading.
Subscript k (e.g. x_k) relates to the kth time interval.

A	area of real section
$A_{\text{t,tr}}$	area of TTS
$b(y)$	width of section
C	specific creep
$\{D\}$	generalised nodal displacements
E and $E(t)$	elastic modulus
$\{\bar{\boldsymbol{F}}\}$	generalised member end forces about actual section
$\{\Delta\bar{\boldsymbol{F}}_{k,\text{fix}}\}$	increment of thermal fixed-end forces in the kth interval
$\{\Delta\bar{\boldsymbol{F}}_{k,\text{nod}}\}$	increment of thermal member end forces caused by nodal loads in the kth interval
$\{\bar{\boldsymbol{F}}^1_{\text{ref}}\}, \{\bar{\boldsymbol{F}}^2_{\text{ref}}\}$	the first and second part of member forces in the reference interval
G	position of centroidal axis of actual section
$G_{\text{t,tr}}$	position of centroidal axis of TTS
h	depth of section
I	second moment of area about the centroidal axis of actual section
$I_{\text{t,tr}}$	second moment of area of TTS about the centroidal axis of TTS
$[\boldsymbol{K}]$	total stiffness matrix
$[\boldsymbol{K}_{\text{t,tr}}]$	total stiffness matrix of TTS
$[\boldsymbol{k}'_{\text{t,tr}}]$	member stiffness matrix of TTS in LCS
$\boldsymbol{M}$	bending moment
$m_{\text{t}}(y)$	modular ratio due to temperature
O	position of centroidal axis of the actual section
$\{\boldsymbol{P}'\}$	generalised total nodal loads of TTS
$T(y)$	temperature at depth y
t	time
t^*	pseudo-time
t_k	length of time for kth interval
t_0	time of loading
$\boldsymbol{X}'_i, \boldsymbol{Y}'_i, \boldsymbol{M}'_i$	axial force, vertical force and moment at end i in LCS (TTS)
$x - y$	global coordinate system
$\bar{x} - \bar{y}$	local coordinate system
$x' - y'$	local coordinate system (TTS)
y	position in a section measured from the bottom surface
$\Gamma(y)$, Γ	normalising creep–temperature function
$\Gamma_{\text{av}}(y)$, Γ_{av}	average normalising creep–temperature function
$\boldsymbol{\varepsilon}$	strain
$\dot{\boldsymbol{\varepsilon}}_{\text{av}}$	average rate of strain for the complete cycle
$\boldsymbol{\kappa}$	curvature
$\Delta\boldsymbol{\kappa}_i$	increment of curvature
$\boldsymbol{\sigma}$, $\boldsymbol{\sigma}(y)$	stress
$\boldsymbol{\sigma}_{\text{cr}}$	stress caused by creep
$\boldsymbol{\sigma}_{k,\text{free}}(y)$	free stress
$\boldsymbol{\sigma}^1_{\text{ref}}(y)$, $\boldsymbol{\sigma}^2_{\text{ref}}(y)$	first part and second part of stress in the reference interval
$\boldsymbol{\sigma}_{k,\text{self}}(y)$	self-equilibrating stress
$\boldsymbol{\sigma}_{\text{th}}$	total thermal stress
ϕ	creep coefficient

1. INTRODUCTION

When an indeterminate structure is built sequentially, trapped moments are induced in the structure so that the bending moment differs from that which would occur if the structure were built at one time. Creep effects are important for the design of sequentially built prestressed concrete structures, since they alter these trapped moments.

Designers do not need to know the *detailed* variation of stress at any particular time, and certainly do not want to perform time-dependent creep calculations. Even if such calculations could be performed easily, the data on concrete properties and temperature variations are unknown and unknowable at the time of design. What *would* be useful is information about the *range* of bending moments to which the structure can be subjected; provided the structure is satisfactory at the limits of the range, the intermediate behaviour is of no concern.

In the usual design process, the creep effects are considered as uniform through the depth of the beam and the effect of creep is to move the dead load bending moments to those that would have occurred if the beam had been built in one stage; this will be termed the *monolithic moment diagram*.[1,2] The 'as-built' moment distribution and the 'monolithic' moment diagram thus serve as bounds for the dead-load response. Thermal effects are considered separately, as a purely elastic structural response to temperature.

However, it is known that the rate of creep is dependent on the temperature.[3] Since the temperature distribution is usually non-uniform through the depth of the section, the rate of creep at each fibre is different and secondary forces caused by creep are different from the uniform creep effects. The stress distribution through the depth will also be non-linear because of the introduction of self-equilibrating stresses.[4]

England identified steady-state creep as the condition when creep is continuing, albeit slowly, with no change in stress.[4] A similar condition can be identified for states in which the temperature changes cyclically; when the stress state is the same at the beginning and end of each cycle the structure can be said to have reached its steady state. Numerical results show that the steady state is the limit when evaluating total creep effects, but most studies have been conducted for structures built in one stage.[4–6] For sequentially built structures, it is necessary to derive an analysis that can evaluate total thermal-creep effects safely without doing detailed time-dependent analysis from the construction stage to service life.

The theory of thermal creep was developed initially for nuclear power plant structures.[3,4,7] Their operating temperature is higher than for bridges (typically 20–120°C) and a simplified creep–temperature function was assumed that was reasonable over that range. In bridges, the temperature range is lower (typically 0–30°C), but there will be a small temperature crossfall over the depth caused by inward solar radiation on the top and outward thermal radiation on the underside. The soffit is typically about 10–15°C cooler than the top surface.[8] It will be shown in this work that this small temperature variation, and the exact form of the creep–temperature function, are important factors in determining the final moment diagram.

Bridges are directly subjected to cyclic temperature variations. For the consideration of creep effects, daily variations (for younger concrete) and seasonal variations (for older concrete) are of importance. Xu[8] showed that the temperature distribution through the depth of a section can be considered as linear for the purpose of thermal-creep analysis, even when there are short-term non-linear variations at the surfaces.

2. TIME-DEPENDENT THERMAL-CREEP ANALYSIS

Time-dependent thermal-creep analysis can give the detailed variation of the beam behaviour with time, although it is too complex for day-to-day use. In the rate-of-creep method, the creep strain rate is given by

$$\frac{\mathrm{d}\boldsymbol{\varepsilon}}{\mathrm{d}t} = \frac{1}{E}\frac{\mathrm{d}\boldsymbol{\sigma}}{\mathrm{d}t} + \frac{\boldsymbol{\sigma}}{E}\frac{\mathrm{d}\phi}{\mathrm{d}t} \tag{1}$$

England[9] introduced the concept of pseudo-time. He assumed that by rescaling time he could separate the effects of temperature and load history, so that the specific creep C could be separated in product form as

$$C(T, t, t_0) = \Gamma[T(y)] \times t^*(t, t_0) \tag{2}$$

Here, $\Gamma[T(y)]$ is the normalising creep–temperature function and $t^*(t, t_0)$ is pseudo-time. It then follows from the definition of specific creep that pseudo-time must be a function of the concrete properties (E and Γ) and the loading history (contained within ϕ). It has dimensions MPa^{-1}.

$$t^*(t, t_0) = \frac{\phi(T = 20, t, t_0)}{E(t_0) \times \Gamma(T = 20)} \tag{3}$$

By introducing the relationship shown in equation (3), England[7] showed that equation (1) can be further simplified as

$$\frac{\mathrm{d}\boldsymbol{\varepsilon}}{\mathrm{d}t^*} = \frac{1}{E}\frac{\mathrm{d}\boldsymbol{\sigma}}{\mathrm{d}t^*} + \boldsymbol{\sigma} \times \Gamma \tag{4}$$

Integrating equation (4), the increment of strain in a given real time interval from t_1 to t_2 is expressed as

$$\Delta\boldsymbol{\varepsilon} = \frac{\Delta\boldsymbol{\sigma}(t_1)}{E(t_1)} + \boldsymbol{\sigma}(t_1) \times \Gamma[T(y)] \times \Delta t^*(t_2, t_1) \tag{5}$$

If the displacement of a fibre is restrained, as in a stress-relaxation test, the rate of strain will be zero, so

$$\frac{1}{E(t_0)}\frac{\mathrm{d}\boldsymbol{\sigma}(t)}{\mathrm{d}t^*} + \boldsymbol{\sigma}(t) \times \Gamma[T(y)] = 0 \tag{6}$$

Solving the differential equation (6) and noticing that the initial stress is $\boldsymbol{\sigma}(t_1)$, the stress at the end of the time interval is

$$\boldsymbol{\sigma}(t) = \boldsymbol{\sigma}(t_1) \exp\{-E(t_1)\Gamma[T(y)]\Delta t^*(t_2, t_1)\} \tag{7}$$

where

$$\Delta t^*(t_2, t_1) = t^*(t_2, t_0) - t^*(t_1, t_0) \tag{8}$$

Equation (7) shows that creep effects exponentially decay but with a time constant in pseudo-time that is a function of both Young's modulus E and the creep–temperature function Γ, both of which are variables.

The structural analysis of time-dependent, thermal-creep effects is based here on the displacement method. The length of time to be considered is divided into many short time intervals.

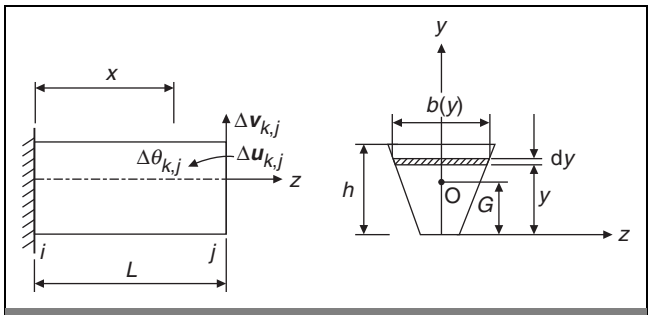

Fig. 1. Basic cantilever element

The structure is divided into several elements. Each element is first considered as a cantilever, as indicated in Fig. 1.

The basic cantilever member is statically determinate, so the effects of creep will induce displacements at the free end but will not change member end forces. The increment of hypothetical free strain at each fibre of a section during the kth interval decays with the same time constant as in equation (7)

$$\Delta\boldsymbol{\varepsilon}_{k,\text{free}}(y) = \frac{\boldsymbol{\sigma}_{t_{k-1}}(y)\{1 - \exp[-E(t_{k-1})\Gamma[T(y)]\Delta t^*(t_k, t_{k-1})]\}}{E(t_{k-1})} \quad (9)$$

According to the assumption of plane sections, the strain distribution through the depth must be linear. If the hypothetical free change of strain determined in equation (9) is artificially prevented in the interval k, the increment of stress introduced gradually during this interval will be

$$\Delta\boldsymbol{\sigma}_{k,\text{free}}(y) = -E(t_{k-1})\Delta\boldsymbol{\varepsilon}_{k,\text{free}}(y) \quad (10)$$

These stress increments can be integrated through the depth of the beam to get the resultant force and moment. To remove the artificial restraint, equal and opposite stress resultants can be applied, which will cause stresses $\Delta\boldsymbol{\sigma}_{k,\text{a}}(y)$. These should be added to the stresses from equation (10) to get the final stress change in the increment.

$$\Delta\boldsymbol{\sigma}_{k,\text{self}}(y) = \Delta\boldsymbol{\sigma}_{k,\text{a}}(y) + \Delta\boldsymbol{\sigma}_{k,\text{free}}(y) \quad (11)$$

At the start of the kth interval, the stress distribution and the temperature distribution are known, so the increment of element end forces $\{\Delta\bar{\boldsymbol{F}}_{k,\text{fix}}\}$, when the ends are restrained, can be determined easily using virtual work. These are transformed from the local to global coordinate systems and added to the nodal loads $\{\Delta\bar{\boldsymbol{F}}_{k,\text{nod}}\}$.

$$\{\Delta\bar{\boldsymbol{F}}_{\text{cr},k}\} = \{\Delta\bar{\boldsymbol{F}}_{k,\text{nod}}\} + \{\Delta\bar{\boldsymbol{F}}_{k,\text{fix}}\} \quad (12)$$

The stresses caused by these end forces are added to the self-equilibrating stresses

$$\Delta\boldsymbol{\sigma}_{\text{cr},k}(y) = \Delta\boldsymbol{\sigma}_k(y) + \Delta\boldsymbol{\sigma}_{\text{self}}(y) \quad (13)$$

These nodal forces and local stresses are then summed over all the intervals. Further details of this analysis are presented in Xu.[8]

3. STEADY-STATE ANALYSIS UNDER SUSTAINED TEMPERATURE

The steady-state analysis is much simpler to carry out than the time-dependent analysis. The method has been confirmed and theoretically studied by England and colleagues[3,4,7] most papers use a force method of analysis although displacement analyses are normally used in real applications or for large problems.[10] In this paper, the steady-state analysis is based on the rate-of-displacement theory of creep, which is analogous with the displacement method.

As for the time-dependent analysis, the rate of strain is the sum of the rate of elastic strain and the rate of creep strain

$$\dot{\boldsymbol{\varepsilon}} = \dot{\boldsymbol{\varepsilon}}_{\text{e}} + \dot{\boldsymbol{\varepsilon}}_{\text{cr}} = \frac{\dot{\boldsymbol{\sigma}}}{E} + \boldsymbol{\sigma}\Gamma[T(y)] \quad (14)$$

The dot notation indicates differentiation with respect to pseudo-time, t^*. The steady state occurs when the change of stress is zero, so the rate of elastic strain is also zero; the rate of strain is then

$$\dot{\boldsymbol{\varepsilon}} = \dot{\boldsymbol{\varepsilon}}_{\text{cr}} = \boldsymbol{\sigma}\Gamma[T(y)] \quad (15)$$

The steady state found by this analysis implies that no further stress redistribution is taking place, although creep may still be continuing, albeit at a lower rate.

Equation (15) can be thought of as analogous to the relationship between elastic stress and strain

$$\boldsymbol{\varepsilon} = \frac{\boldsymbol{\sigma}}{E} \quad (16)$$

The temperature-related function $\Gamma[T(y)]$ is analogous to $1/E$ in the elastic stress–strain relationship. Based on this idea, the relationship between the rate of displacement and nodal forces can be deduced.

The temperature distribution is usually non-uniform through the depth. The breadth of the section can be adjusted (in analogy with an adjustment for varying E) to produce a *temperature-transformed section* (TTS) which is then used in the structural analysis. Selecting a reference temperature T_{ref} at a particular position, the ratio of $\Gamma[T(y)]$ at other positions through the depth is

$$m_{\text{t}}(y) = \frac{\Gamma(T_{\text{ref}})}{\Gamma[T(y)]} \quad (17)$$

which is effectively the modular ratio that can be used to modify the breadth of the section at depth y (Fig. 2). The geometric properties of the TTS are then calculated in the normal way.

The section properties and $\Gamma(T_{\text{ref}})$ are then used to set up the member stiffness matrix $[\boldsymbol{k}_{\text{t,tr}}]$ and total stiffness matrix $[\boldsymbol{K}_{\text{t,tr}}]$ in the usual way. Due allowance needs to be made for the difference between the global coordinate system (GCS), the local coordinate systems (LCSs) about the centroidal axes of the physical section, and also that of the TTS.

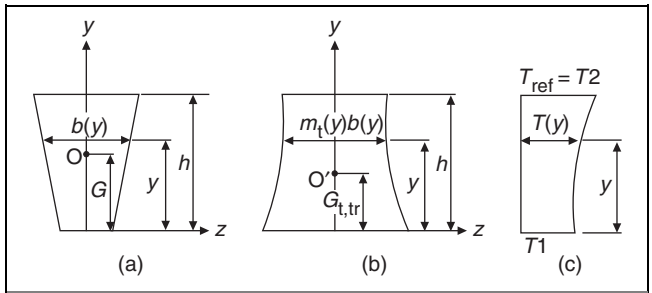

Fig. 2. Relationship between actual section and TTS. (a) Actual section; (b) TTS; (c) temperature distribution

As is usual in the stiffness method, the result is a relationship between the displacement and nodal loads, but in the present case the expression is in terms of rate of displacement

$$\{\dot{D}\} = [\boldsymbol{K}_{\mathrm{t,tr}}]^{-1}\{\boldsymbol{P}'\} \quad (18)$$

where $\{\dot{D}\}$ is rate of nodal displacements and $\{\boldsymbol{P}'\}$ is nodal loads in GCS about the TTS.

The rate of nodal displacement of each element and the element end forces are then found in the normal way. The stress distribution of a section can be calculated from $\{\boldsymbol{F}'\}$ directly, taking account of the equivalent modular ratio. At a depth y the stress is

$$\boldsymbol{\sigma}_i(y) = \frac{\Gamma(T_{\mathrm{ref}})}{\Gamma[T(y)]} \times \left[\frac{\boldsymbol{X}'_i}{A_{\mathrm{t,tr}}} - \frac{\boldsymbol{M}'_i}{I_{\mathrm{t,tr}}}(y - G_{\mathrm{t,tr}})\right] \quad (19)$$

Full details of the implementation of the method are given in Xu,[8] where it is applied to beams; a slightly more sophisticated analysis would be needed for frames where the centroidal axes of beams and columns might not meet at a point after temperature transformations had been applied.

4. STEADY STATE UNDER CYCLIC TEMPERATURES

England *et al.*[5] proposed a method to analyse the steady state under cyclic temperature variations. A complete temperature cycle, as in Fig. 3, is assumed to be broken up into a number of intervals, in each of which the temperature remains constant. Once the steady state has been reached it is assumed that the stresses in the various intervals differ only by a set of thermal stresses. Real time t is used to replace pseudo-time, t^*, for simplicity, since the relationship between real time and pseudo-time is almost linear once the steady state has been reached. In the present application, the first interval in a cycle is assumed to be the reference interval. England *et al.*[5] and Xu[8] show that the stress state in the reference interval is the sum of two parts

$$\boldsymbol{\sigma}_{\mathrm{ref}}(y) = \boldsymbol{\sigma}^1_{\mathrm{ref}}(y) + \boldsymbol{\sigma}^2_{\mathrm{ref}}(y) \quad (20)$$

where

$$\boldsymbol{\sigma}^1_{\mathrm{ref}}(y) = \frac{\dot{\boldsymbol{\varepsilon}}_{\mathrm{av}}(y)}{\Gamma_{\mathrm{av}}(y)} \quad (21)$$

$$\boldsymbol{\sigma}^2_{\mathrm{ref}}(y) = \frac{\sum_{k=1}^{n} \boldsymbol{\sigma}_{\mathrm{th}k}(y) t_k \Gamma[T_k(y)]}{\Gamma_{\mathrm{av}}(y) \sum_{k=1}^{n} t_k} \quad (22)$$

$$\Gamma_{\mathrm{av}}(y) = \frac{\sum_{k=1}^{n} t_k \Gamma[T_k(y)]}{\sum_{k=1}^{n} t_k} \quad (23)$$

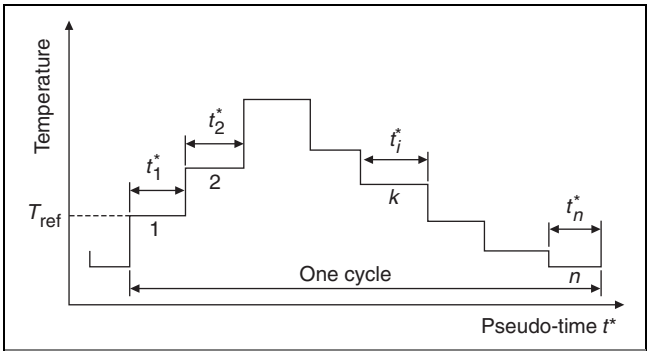

Fig. 3. Temperature variations with respect to pseudo-time in a cycle

The relationships in equations (21) and (22) can be used for structural analysis.[8]

Equation (21) gives the stress in the reference interval caused by the average effect of thermal creep over the cycle; it is similar to equation (15) when $\Gamma_{\mathrm{av}}(y)$ is used as the sustained normalising creep–temperature function. The final element forces caused by equation (21) are $\{\bar{\boldsymbol{F}}^1_{\mathrm{ref}}\}$ and the stress distribution at node i is $\boldsymbol{\sigma}^1_{\mathrm{ref}}(y)$. These values can be calculated by the rate of displacement method in section 3 directly.

Equation (22) represents the stress caused in the reference interval by the variation of temperature over the cycle. $\boldsymbol{\sigma}_{\mathrm{th}k}(y)$ is the elastic thermal stress caused by the change of temperature from the reference interval to interval $\boldsymbol{k}$; the structural analysis is based on the basic cantilever element as before.

The strains at the centroid O at node i induced by equation (22) is

$$\Delta\boldsymbol{\varepsilon}_{\mathrm{o},i} = \int_0^h \frac{\sum_{k=2}^{n} \boldsymbol{\sigma}_{\mathrm{th}k,i}(y) t_k \Gamma[T_k(y)]}{E \times A \times \Gamma_{\mathrm{av}}(y) \sum_{k=1}^{n} t_k} b(y)\mathrm{d}y \quad (24)$$

Similarly, the curvature is

$$\Delta\boldsymbol{\kappa}_i = \int_0^h \frac{\sum_{k=2}^{n} \boldsymbol{\sigma}_{\mathrm{th}k,i}(y) t_k \Gamma[T_k(y)]}{E \times I \times \Gamma_{\mathrm{av}}(y) \sum_{k=1}^{n} t_k} b(y)(y - G)\mathrm{d}y \quad (25)$$

If the fibre at the depth y is not restrained, the corresponding stress at node i is

$$\boldsymbol{\sigma}_{\mathrm{free},i}(y) = \frac{\sum_{k=2}^{n} \boldsymbol{\sigma}_{\mathrm{th}k,i}(y) t_k \Gamma[T_k(y)]}{\Gamma_{\mathrm{av}}(y) \sum_{k=1}^{n} t_k} \quad (26)$$

The section is assumed to remain plane, so a self-equilibrating stress is needed to adjust the strain. At depth y, this can be expressed as

$$\Delta\boldsymbol{\sigma}_{\mathrm{self},i}(y) = \boldsymbol{\sigma}_{\mathrm{free},i}(y) - E\Delta\boldsymbol{\kappa}_i(y - G) - E\Delta\boldsymbol{\varepsilon}_{\mathrm{o}} \quad (27)$$

The axial strain $\Delta\boldsymbol{\varepsilon}_{\mathrm{o}}(x)$ and curvature $\Delta\boldsymbol{\kappa}(x)$ vary linearly between the two ends. The displacements at the free end can be calculated by integrating along the length of the element. Using the same restrain–release procedure as before, the element end forces, $\{\bar{\boldsymbol{F}}^2_{\mathrm{ref}}\}$, caused by equation (22) can be solved by structural analysis about the actual section. The stress distribution at node i calculated by the structural analysis, $\Delta\boldsymbol{\sigma}_{\mathrm{ref},i}$ is linearly distributed through the depth. The total stress distribution at end i is then

$$\boldsymbol{\sigma}^2_{\mathrm{ref},i}(y) = \Delta\boldsymbol{\sigma}_{\mathrm{ref},i} + \Delta\boldsymbol{\sigma}_{\mathrm{self},i}(y) \quad (28)$$

The final element end forces and stress distributions are thus

$$\{\bar{\boldsymbol{F}}_{\mathrm{ref}}\} = \{\bar{\boldsymbol{F}}^1_{\mathrm{ref}}\} + \{\bar{\boldsymbol{F}}^2_{\mathrm{ref}}\} \quad (29)$$

$$\boldsymbol{\sigma}_{\mathrm{ref},i}(y) = \boldsymbol{\sigma}^1_{\mathrm{ref},i}(y) + \boldsymbol{\sigma}^2_{\mathrm{ref},i}(y) \quad (30)$$

5. NORMALISING CREEP–TEMPERATURE FUNCTION

England[9] showed that if incorporating temperature effects, the strain caused by creep is

$$\boldsymbol{\varepsilon}_{\mathrm{cr}}(t, t_0, T) = \boldsymbol{\sigma}(t_0)\Gamma(T)t^*(t, t_0) \quad (31)$$

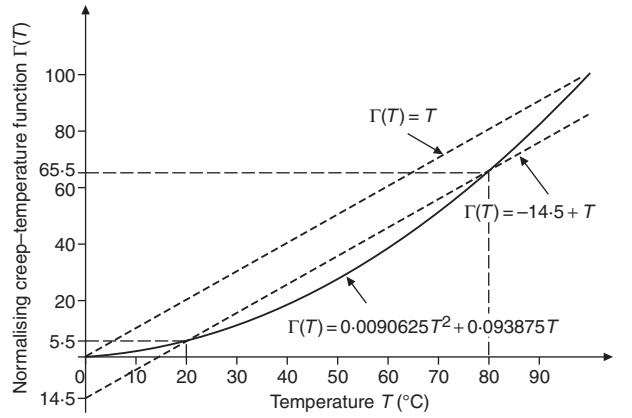

Fig. 4. Comparison of various normalising creep–temperature functions

In several papers,[5,6] this creep–temperature function $\Gamma(T)$ was taken as the value of temperature in °C directly. This will be termed the *proportional form* of the creep–temperature function.

$$\Gamma(T) = T \quad (32)$$

However, experimental results show that $\Gamma(T)$ is a more complex function and should be approximated as a parabolic expression,[5] but that reference did not propose a detailed equation. Hannant's experimental work[11] showed that $\Gamma(T)$ can be approximated as linear when the temperature is between 20 and 80°C.[6]

$$\Gamma(T) = -14{\cdot}5 + T \quad (33)$$

Equations (32) and (33) may be relevant for nuclear pressure vessels, in which temperatures can be quite high, but for bridges temperatures often fall below 20°C. If $\Gamma(T)$ is assumed to be parabolic, the function can be found by assuming that $\Gamma(0) = 0$ because water freezes and no creep occurs, and taking

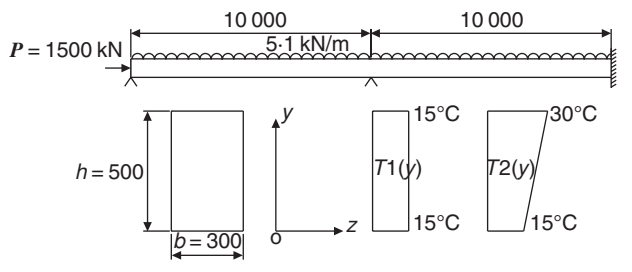

Fig. 5. Basic structure and temperature crossfalls (all units in mm)

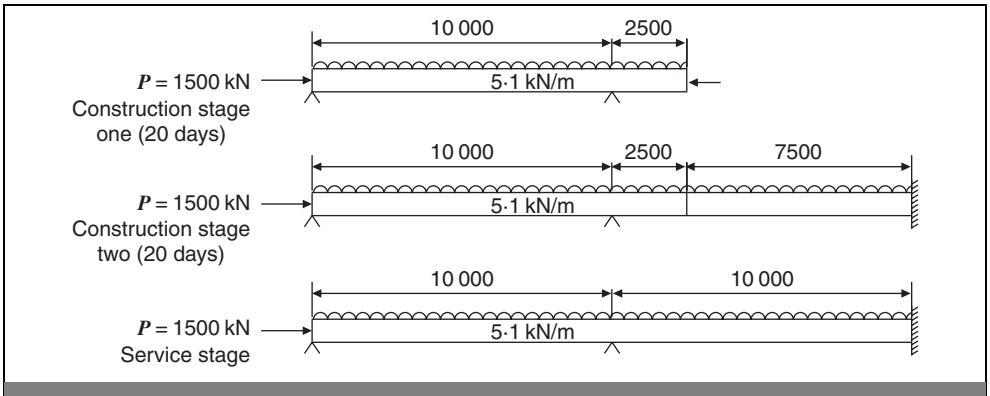

Fig. 6. Construction sequence (all units in mm)

$\Gamma(20) = 5{\cdot}5$ and $\Gamma(80) = 74{\cdot}5$ from equation (31). The creep–temperature function is then

$$\Gamma(T) = 0{\cdot}0090625T^2 + 0{\cdot}093875T \quad (34)$$

The three versions of the creep–temperature function are shown in Fig. 4.

6. NUMERICAL EXAMPLES

The following numerical examples are designed to show the effects of changing the form of the creep–temperature function, and also of taking into account sequential construction. In all cases, the concrete is assumed to have a cube strength of 40 MPa, with the elastic modulus E and creep function ϕ taken from the GTG-9 report.[12] The coefficient of thermal expansion is taken as $12 \times 10^{-6}/°C$.

The basic structural dimensions, as shown in Fig. 5, are taken from England *et al.*[5] so that a direct comparison can be made with the earlier work. The construction sequence is indicated in Fig. 6. Because thermal effects are being taken into account, an assumption must be made about the temperature at which the structure was built; it is assumed here that the structure was completed, stress-free, at 15°C. The examples from England *et al.*[5] were obtained at higher temperatures using the force method; they have been analysed again using the present stiffness formulation, as a check, and the results agree. The examples presented here are all calculated for typical bridge temperatures.

6.1. Effect of changing form of $\Gamma(T)$

The first analysis of the structure is carried out on the assumption that it has been built monolithically, at the constant stress-free temperature $T1$, and is completed when the concrete is 20 days old. The temperature then changes to the distribution $T2$. Although slightly artificial this allows the effect of changing the creep–temperature function to be studied. If using the proportional function (equation (32)) for $\Gamma(T)$, the variation of bending moment is as shown in Fig. 7. The bending moment diagram on completion is shown as the 20-day curve; because the structure was built monolithically, this is the bending moment diagram that a simple analysis of the complete structure under its dead load would produce. In the assumed scenario, the temperature immediately changes to $T2$; the top is hotter than the bottom, so the beam tends to hog due to thermal expansion. This hogging is resisted by the indeterminate restraints, so sagging bending moments are induced. The structure then immediately starts to creep; since the top is warmer, creep takes place more rapidly there, so the beam tries to sag, thus inducing hogging restraint moments, and the bending moment diagram eventually reaches the steady-state prediction, which is thus an upper-bound on the bending moments.

The various curves on Fig. 7 all relate to the same dead load, so they differ only by changes in

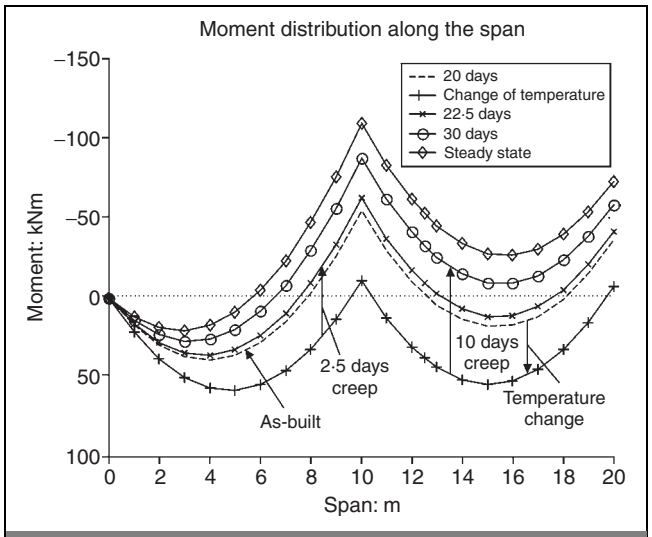

Fig. 7. Bending moment diagram for monolithic construction (linear creep–temperature function)

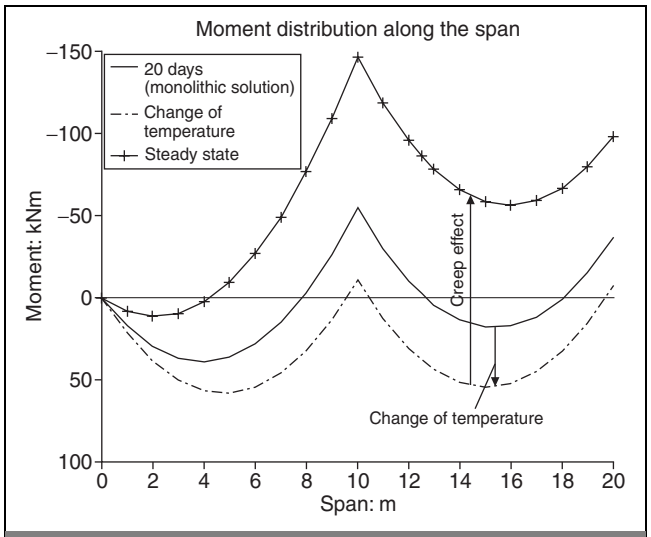

Fig. 9. Bending moment diagram for monolithic construction (parabolic creep–temperature function)

the indeterminate support reactions. Fig. 8 shows the change in the intermediate support reaction with time, which shows more clearly the speed with which creep acts. The monolithic (20-day) value (point A in Fig. 8) alters immediately to B when the temperature change takes effect. Creep then starts and the reactions and bending moments move towards the steady-state solution (C in Fig. 8). The analysis was stopped after 1000 days when the difference from the asymptote is insignificant.

The analysis is then repeated, using the parabolic form (equation (34)) as the normalising creep–temperature function; the variation of bending moment and the internal support reaction with time are illustrated in Figs 9 and 10, respectively. The monolithic and temperature bending moments are as in the previous example, but the steady-state solution is different. Over the temperature ranges considered here (15–30°C), the Γ values are much lower using the parabolic function, so less creep can be expected to occur. However, the ratio between $\Gamma(30)$ and $\Gamma(15)$ is higher with the parabolic variation than with the proportional function. This means that the TTS differs more from the notional shape of the section as shown in Fig. 11. Taken together, these effects mean that the steady-state solution differs more from the monolithic solution, but the structure takes longer to creep towards it, taking about 400 days to reach 90% of the total creep effects in Fig. 10, compared with only 55 days in Fig. 8. This difference is significant, since the shorter period is likely to occur while the structure is still under construction and it is unlikely that live loads will be acting while creep is ongoing. For the longer period, the structure will still be creeping when the bridge is open to traffic. Using different creep–temperature functions can result in very different solutions; for example, the hogging bending moments near the internal support and the fixed end are much higher in Fig. 9 than in Fig. 7.

All subsequent analyses will be performed with the parabolic form of $\Gamma(T)$.

6.2. Effect of staged construction

The structure is now reanalysed, this time on the assumption that it is built in two stages, as shown in Fig. 6. The first stage, which becomes self-supporting at 20 days, is statically

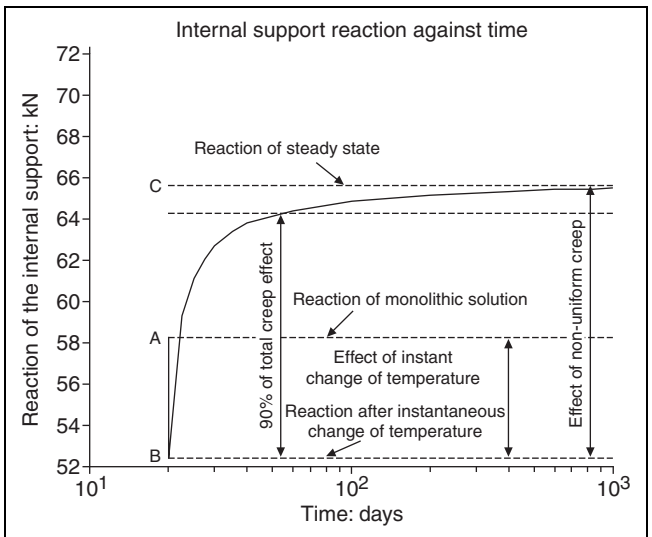

Fig. 8. Change of reaction of the internal support with time

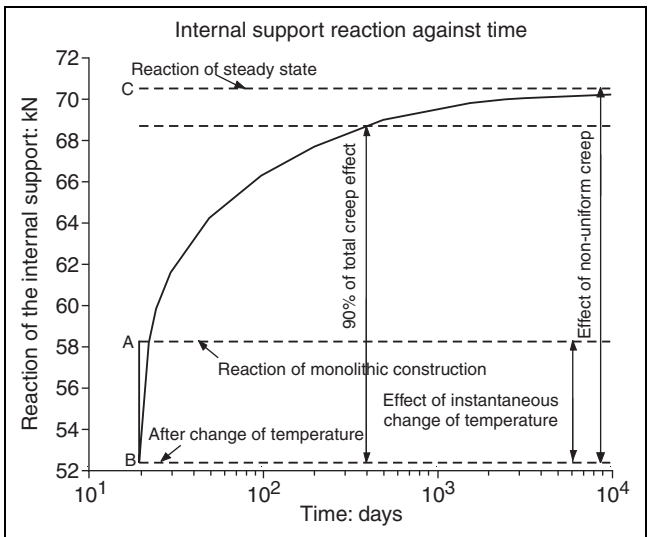

Fig. 10. Change of reaction of the internal support with time

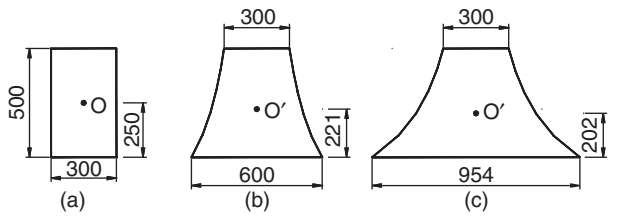

Fig. 11. Actual section and temperature transformed sections. (a) Actual section; (b) TTS-proportional; (c) TTS-parabolic (all units in mm)

determinate, so although it creeps, no change in the bending moments occurs. After a further 20 days, the second stage is completed and the structure becomes indeterminate. The variations of bending moment diagram and internal support reaction with time are indicated in Figs 12 and 13, respectively. The difference between the 40-day curve and the monolithic bending moment is the trapped moment induced by the construction sequence.

From Figs 12 and 13, it can be observed that the steady-state solution can still serve as an asymptote, although it takes much longer to reach it. This is because much of the creep of the concrete in phase 1 has already occurred before the structure became indeterminate; it now takes about 1100 days for 90% of the total creep effect to take place, and even after 10 000 days the asymptote has not been reached. Under these circumstances the designer *must* assume that the live load can act on the structure both before and after creep has taken place. This will have the effect of increasing the *range* of bending moments for which the structure must be designed, and may well require a larger cross-section.

It should also be noticed in Fig. 13 that the reaction of the internal support does not move towards the steady-state solution at the beginning of the period of creep (from the 40 to 42·5 days). This behaviour may be significant in some cases, since it implies that the concretes of two different ages are working against each other, which can lead, in some cases, to moments that lie outside the bounds. This is most likely to occur when short lengths of *in situ* concrete are used to join together longer structural elements which had been in place for some time, and

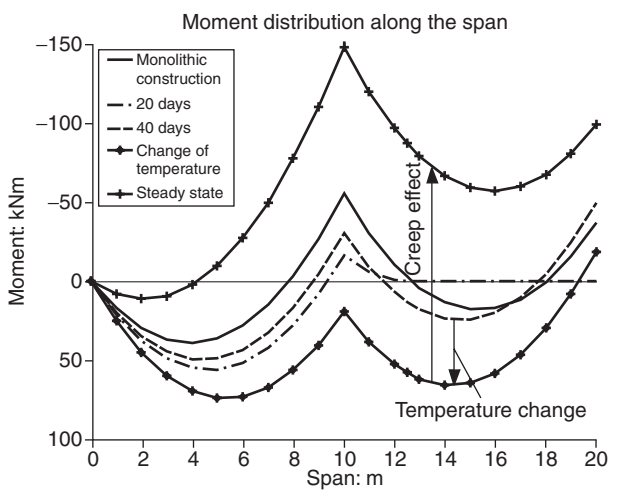

Fig. 12. Bending moment diagram for sequential construction

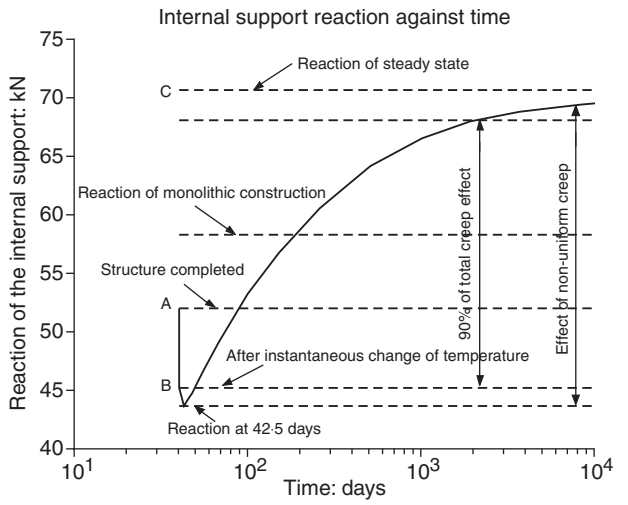

Fig. 13. Change of reaction of the internal support with time-sequential construction

which had hitherto been statically determinate. Balanced cantilever construction springs to mind, for example, where short lengths of *in situ* concrete are used to add continuity to the determinate pier sections.

6.3. Effect of temperature cycling

In this example, the basic structure and temperature crossfalls are taken as the same in Figs 5 and 6. The structure is assumed to sustain temperature crossfalls cycling from $T1$ to $T2$, with equal periods of time spent at each temperature. It is accepted that these values are entirely artificial and arbitrary, but they were chosen to represent a case where the top of the beam is periodically warmer than the soffit. Results that are similar in principle have been obtained for other temperature ranges and frequencies.

The structure is first analysed on the assumption that it is built monolithically. Temperature variations with time are indicated in Figs 14 and 15. A cyclic steady-state analysis is carried out, from

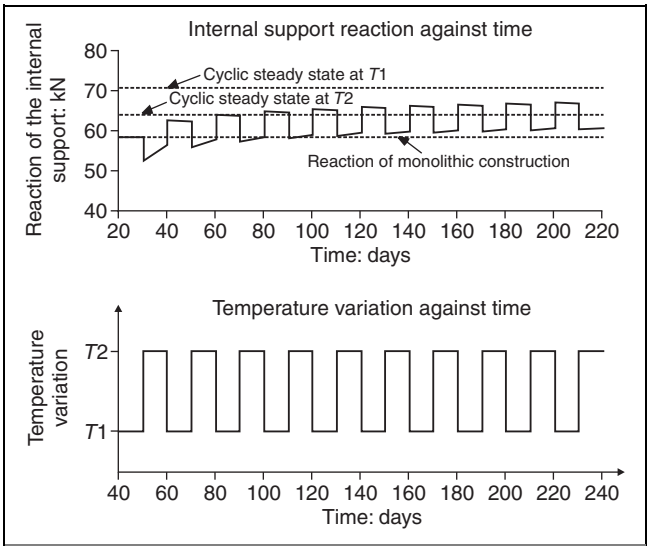

Fig. 14. Change of the internal support reaction with time of the monolithic construction (soon after construction)

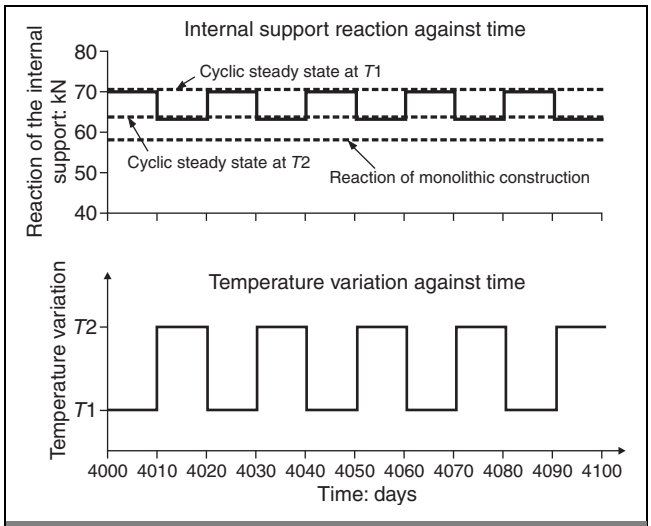

Fig. 15. Change of the internal support reaction with time of the monolithic construction (long after construction)

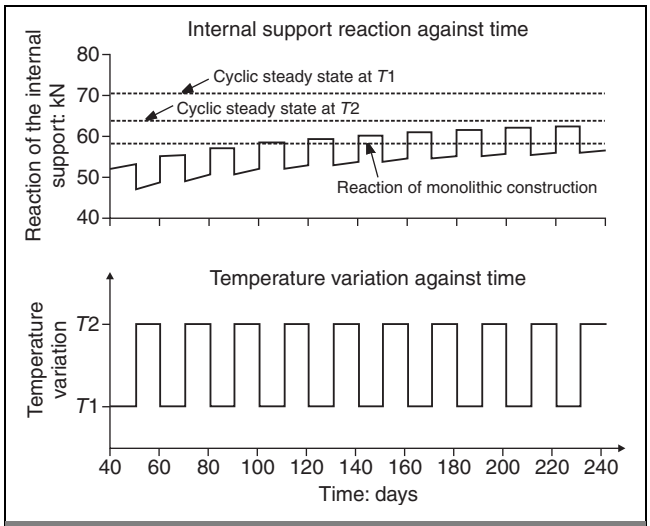

Fig. 17. Change of the internal support reaction with time (soon after construction)

which the eventual response under $T1$ and $T2$ can be calculated. The bending moment diagrams for this range are shown in Fig. 16.

The change in internal support reaction for the first few cycles is shown in Fig. 14, when significant creep is taking place, and for the later cycles in Fig. 15, when creep rates are much reduced. It can be observed that the bending moment diagrams and support reactions all move towards their corresponding cyclic steady-state values at $T1$ and $T2$, respectively.

6.4. Cyclic temperature and staged construction

If the structure is built in two stages as in Fig. 6 and sustains the cycling temperature variations as in Figs 17 and 18 during the service life, the structural behaviour is similar to the previous example, but the effect of the staged construction is to slow down the creep effects and it takes much longer for the structure to reach its asymptotic behaviour; nevertheless, the steady-state behaviour still represents the asymptote to which the system is converging.

7. CONCLUSIONS

The paper has shown that the displacement method can be used to determine creep effects in statically indeterminate structures, which makes it simple to combine creep analysis and normal elastic analysis. The following conclusions have been drawn.

(*a*) The selection of an appropriate normalising creep–temperature function is important and can have a significant effect on the resulting bending moments. It is recommended that a parabolic expression be used; the simplified form, which uses the magnitude of temperature directly, may not produce safe results for the structure under the lower temperatures to which bridges are subjected. More experimental work should be done to determine the normalising creep–temperature function for structures under temperature variations between 0 and 40°C.

(*b*) The effect of using the parabolic form of the creep–temperature function is to slow down the rate of creep at normal temperatures, but to increase the eventual effect of

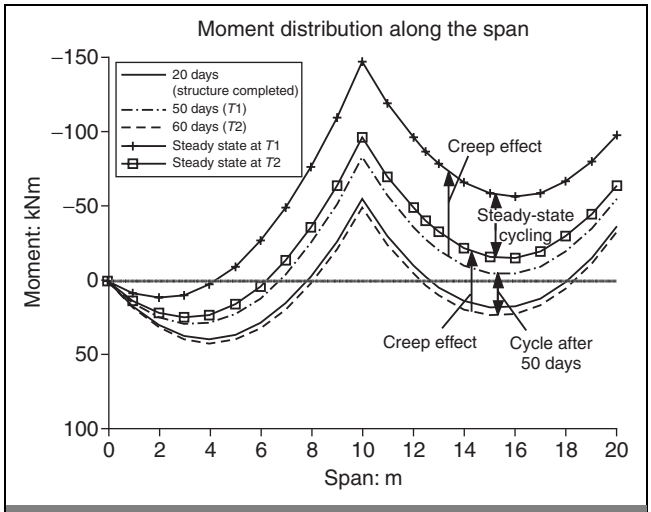

Fig. 16. Bending moment diagram for monolithic construction under cyclic temperatures

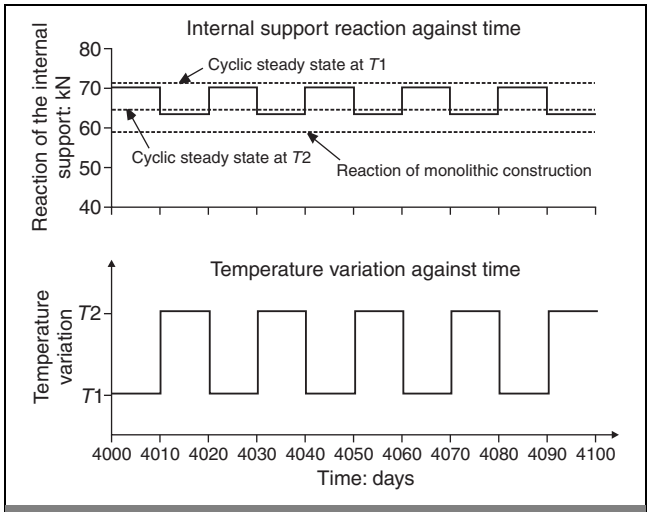

Fig. 18. Change of the internal support reaction with time (well after construction)

the creep caused by the variation of the temperature over the depth of the section.

(*c*) The results of steady-state analysis of the structure under sustained temperature crossfall can be considered as one bound on the dead load bending moment diagram subjected to creep effects for both monolithically and sequentially constructed bridges.

(*d*) The 'as-built' moment diagram can serve as the other bound. The elastic response of the structure to short-term temperature variations should be added to these bounds.

(*e*) The long-term structural response to cyclical temperature variations can also be evaluated by the cyclic steady-state analysis.

(*f*) In the analysis of sequentially built structures, concrete of different ages can work in opposition, which could lead, in some cases, to moments and reactions that lie outside the bounds for both uniform and non-uniform creep analysis. This will be most important when a short *in situ* section is used to add continuity to otherwise statically determinate structures.

(*g*) Thermal creep analysis produces significantly different bending moment and stress distributions when compared with the initial state of the sequentially built structures. This phenomenon must be taken into account in the design.

(*h*) Even for concretes with the same properties, the speed with which creep effects take place is heavily dependent on the construction sequence and the thermal environment.

The analysis presented here has shown that thermal-creep effects may be important in the design of bridges, even when the temperature variation across the section is small; it is clear that a full parametric study of the interaction of these effects with various construction sequences should be carried out.

8. ACKNOWLEDGEMENT

The authors would like to thank Professor George England of Imperial College for his assistance with the study on which this paper is based.

REFERENCES

1. GHALI A. and FARVE R. *Concrete Structures: Stresses and Deformations*, 2nd edn. E & FN Spon, London, 1994.
2. SHUSHKEWICH K. W. Time-dependent analysis of segmental bridges. *Computers and Structures*, 1986, **23**, No. 1, 95–118.
3. ROSS A. D., ENGLAND G. L. and SUAN R. H. Prestressed concrete beams under a sustained temperature crossfall. *Magazine of Concrete Research*, 1965, **17**, No. 52, 117–126.
4. ENGLAND G. L. Steady-state stresses in concrete structures subjected to sustained and cyclically varying temperatures. *Nuclear Engineering and Design*, 1977, **44**, No. 1, 97–107.
5. ENGLAND G. L., CHENG Y. F. and ANDREWS K. R. F. A temperature-creep theory for prestressed concrete continuum and beam structures. *Journal of Thermal Stresses*, 1984, **7**, No. 3–4, 361–381.
6. ROBBERTS J. M. *Behaviour of Integral Bridges Subjected to Nonuniform Temperature Creep and Soil–structure Interaction Loading*. PhD thesis, Department of Civil and Environmental Engineering, Imperial College, London, 2003.
7. ENGLAND G. L. Steady-state stresses in concrete structures subjected to sustained temperatures and loads. *Nuclear Engineering and Design, Part 1*, 1966, **3**, No. 1, 54–65.
8. XU Q. *Effect of Construction Sequence on Creep of Concrete Bridges*. MPhil thesis, Department of Engineering, University of Cambridge, 2004.
9. ENGLAND G. L. Time-dependent stresses in creep-elastic materials: a general method of calculation. *Proceedings of a Conference on Recent Advances in Stress Analysis*, Session 2, Paper 1, Joint British Committee for Stress Analysis, London, March 1968, 8 pp.
10. ENGLAND G. L. and ANDREWS K. R. F. *Temperature–creep Analyses for Beam Structures*. UK Department of Transport Report, Contract No. BE22/2/0112, November 1981.
11. HANNANT D. J. Strain behaviour of concrete up to 95°C under compressive stresses. *Proceedings of a Conference on Prestressed Concrete Pressure Vessels*, Paper C17, Institution of Civil Engineers, London, March 1967, pp. 177–191.
12. GTG-9. Evaluation of the time-dependent behaviour of concrete. *Bulletin d'information 199*, CEB-FIP General Task Group 9, Comité Euro-International du Béton, Lausanne, 1990, pp. 210.